Zeitschrift fuer Medizinische Physik xxx (xxxx) 1–7

Contents lists available at ScienceDirect

Zeitschrift fuer Medizinische Physik

journal homepage: www.elsevier.com

Semi-automated bone tracking in dynamic CINE MRI during controlled knee motion

A. Nepal [a], N.M. Brisson [b, c], T.C. Wood [d], G.N. Duda [b, c], J.R. Reichenbach [a], M. Krämer [a, e, *]

[a] Medical Physics Group, Institute of Diagnostic and Interventional Radiology, Jena University Hospital, Friedrich Schiller University Jena, Germany
[b] Julius Wolff Institute, Berlin Institute of Health at Charité – Universitätsmedizin Berlin, Berlin, Germany
[c] Berlin Movement Diagnostics (BeMoveD), Center for Musculoskeletal Surgery, Charité – Universitätsmedizin Berlin, Berlin, Germany
[d] Department of Neuroimaging, Institute of Psychiatry, Psychology & Neuroscience, King's College London, London, UK
[e] Institute of Diagnostic and Interventional Radiology, Jena University Hospital, Friedrich Schiller University Jena, Germany

ARTICLE INFO

Keywords:
Radial golden-angle acquisition
Canny edge detection
CINE MRI reconstruction
Knee osteokinematics

ABSTRACT

Purpose: Dynamic magnetic resonance imaging (MRI) enables in vivo imaging of bone motion during knee movement, but quantifying joint kinematics from these images remains technically challenging due to image quality trade-offs inherent in dynamic acquisition sequences. We aimed to develop a semi-automated pipeline for tracking femoral and tibial motion from sagittal plane CINE MRI during active knee flexion and extension. The performance of the method was evaluated by quantifying: (i) bone boundary alignment error, (ii) frame segmentation processing time, and (iii) consistency of derived osteokinematic parameters, with the latter two compared against manual segmentation.

Methods: The presented algorithm combines Canny edge detection and connected-component labeling with frame-to-frame transformation optimization to track bone boundaries. The approach was validated in five healthy volunteers performing controlled knee flexion and extension using a dedicated MRI-compatible device. The relative bone displacements measured using the semi-automated approach were qualitatively compared to that from manual segmentation. All bone displacements were defined in the two-dimensional (2D) image coordinate system, with the centroid of the tibial segment tracked relative to the centroid of the femoral segment in the horizontal and vertical directions.

Results: The semi-automated tracking method achieved an average alignment error of 0.40 ± 0.02 mm for both bones, with processing time reduced from approximately 15 minutes for manual segmentation to less than 5 minutes for semi-automated segmentation per dataset. Both approaches showed similar relative bone motion patterns, with horizontal displacement of the tibia with respect to the femur ranging between 8 and 28 mm and vertical displacement remaining relatively constant at around 57 mm through the knee motion cycle. Further analysis revealed that the semi-automated method demonstrated improved precision with smaller standard deviations (SDs) in displacement measurements compared to the manual approach, with horizontal displacements of 1.7–2.7 mm vs. 2.2–3.3 mm and vertical displacements of 0.7–1.2 mm vs. 0.9–1.7 mm.

Conclusion: These results demonstrate the potential of the semi-automated method for reliable and time-efficient quantification of relative bone positions during volitional knee motion in dynamic MRI protocols. The shorter processing time and the demonstrated reliability of the semi-automated method support its utility for analyzing dynamic MRI data.

1. Introduction

Osteokinematics describes the motion of the bones as rigid bodies around a joint that produces physiologic or voluntary movements [1]. In the context of the knee joint, studying the relative motion between the tibia and femur during movement is essential for understanding normal knee function, diagnosing pathological conditions, and improving surgical techniques including prosthetic design [2–4]. An enhanced

* Corresponding author at: Medical Physics Group, Institute of Diagnostic and Interventional Radiology, Jena University Hospital, Philosophenweg 3, D-07443 Jena, Germany

E-mail addresses: aayush.nepal@uni-jena.de (A. Nepal), nicholas.brisson@charite.de (N.M. Brisson), tobias.wood@kcl.ac.uk (T.C. Wood), georg.duda@charite.de (G.N. Duda), Juergen.Reichenbach@med.uni-jena.de (J.R. Reichenbach), martin.kraemer@med.uni-jena.de (M. Krämer).

https://doi.org/10.1016/j.zemedi.2025.06.005
Received 27 March 2025; Accepted 25 June 2025
0939-3889/

understanding of osteokinematics can also help in optimizing surgical techniques for ligament reconstruction, developing rehabilitation protocols, or evaluating the quality of treatment outcomes [5–7]. Accurate assessment of osteokinematics aids in diagnosing and treating various knee disorders involving altered joint biomechanics, including ligament injuries, which can lead to joint instability syndromes, altered ambulatory mechanics, and joint tissue degradation (e.g., osteoarthritis) [8–10]. These disorders can also result from or cause joint malalignment, altered congruency of articulating surfaces, increased joint laxity and/or decreased dynamic joint stability, which can all be better understood through detailed analysis of bone motion patterns [11–13].

So far, MRI has been used to statically analyze the structures inside the body non-invasively. However, dynamics is key to understanding physiology and pathological changes. Dynamic MRI represents a promising tool for studying in vivo knee motion [14]. While several dynamic MRI techniques, including real-time MRI [15,16], CINE MRI [17,18], and CINE phase contrast MRI [19,20], can effectively visualize knee movement, quantifying osteokinematics from these scans presents significant challenges. Dynamic MRI sequences necessarily trade off spatial resolution and image quality to achieve temporal resolution suitable for time-resolved images of joint motion. For methods aiming to track bone motion across MRI frames, one common approach is to use high-resolution static reference scans that must be manually segmented to create detailed bone models, which are then registered to the lower-resolution dynamic frames [19–21]. However, this method increases workflow complexity and data processing time. An alternative method is landmark-based tracking, where anatomical points are manually identified and tracked through subsequent frames using template matching, allowing for direct frame-to-frame motion estimation. However, this approach relies on discrete landmarks rather than utilizing the entire bone boundary information [16], making the bone tracking more vulnerable to identification errors. Such inaccuracies in anatomical landmark identification have been shown to propagate into joint kinematics outcomes [22].

The primary aim of this work was to develop a semi-automated pipeline to consistently track the bones of the knee joint (tibia and femur) using sagittal plane CINE MRI images acquired during controlled, active knee flexion and extension using a custom MRI-compatible knee motion and loading device. Our approach combines Canny edge detection [23] and connected-component labeling [24] with frame-to-frame transformation optimization to track the bone segments across frames, enabling quantification of their relative horizontal and vertical displacements. Unlike methods requiring three-dimensional bone models or landmark-based tracking, our technique relies on the entire bone contour for more robust tracking and operates directly on dynamic MRI data without the need for additional static scans, streamlining the analysis process. Secondary aims were (i) to use the processed data to subsequently measure osteokinematics, more specifically, the relative motion between the proximal tibia and distal femur during the knee flexion-extension movement; (ii) to quantify the bone boundary alignment error of our semi-automated approach; and (iii) to compare the processing time between semi-automated and manual segmentation approaches.

2. Material and Methods

2.1. Image Acquisition and Reconstruction

Five healthy volunteers (three males and two females, 24–39 years old, body mass 55–90 kg) participated in this study. This study was approved by the research ethics boards of the Friedrich Schiller University Jena (2021-2275). All participants provided written, informed consent prior to taking part in the study. Dynamic MRI scans were acquired for the left leg of each participant using a 3 T clinical whole-body MRI scanner (MAGNETOM Prisma, Siemens Healthineers).

A custom MRI-safe knee motion and loading device [25] was used to guide planar knee movement during flexion-extension cycles. Images and videos demonstrating the device and participant setup are available in the supplementary materials of reference [25] https://www.sciencedirect.com/science/article/pii/S093938882100115X#upi0005. Participants were positioned supine with their thigh upon a wedge and secured using a strap in such a way that the knee joint center was aligned with the device's axis of rotation, facilitating flexion and extension. The lower leg was fastened to the ankle rest of the leg support using straps attached just proximal to the malleolus. Additional straps were applied around the thigh to minimize unwanted movement. Two flexible 16-channel multifunctional coils (Variety, Noras MRI products GmbH) were positioned around the knee to enable coverage of the entire joint. One coil was positioned beneath the knee, with the posterior surface of the knee resting directly on it. The other coil was wrapped around the anterior surface of the knee, covering the proximal tibia.

During the scan, participants performed controlled extension-flexion cycles of the knee joint to the beat of a metronome (60 beats per minute). Each knee extension-flexion movement cycle was guided by eight metronome beats, with the knee fully flexed at the first beat, fully extended by the fourth beat and fully flexed again by the eighth beat, resulting in 8 seconds per cycle. The total scan duration was 160 seconds, allowing for the acquisition of approximately 20 full knee extension-flexion cycles.

MRI data were acquired using a 2D radial golden-angle gradient echo FLASH sequence [26,27] with the following parameters: echo time of 2.51 ms, flip angle of 8°, field of view of $[192 \times 192 \times 3]$ mm^3, matrix size of $[176 \times 176 \times 1]$, voxel size of $[1.09 \times 1.09 \times 3]$ mm^3, and repetition time of 5.8 ms. This acquisition protocol captured a single 3 mm thick sagittal slice. For each full k-space scan, 276 spokes were acquired, with each spoke consisting of 352 data points. A total of 100 full k-space scans were acquired during the scan session.

This acquisition method enabled CINE MRI by retrospectively sorting the k-space data into discrete knee angle intervals to create a series of images or frames representing the knee at different flexion positions, effectively producing a series of images (or 'cinema') showing the joint motion.

Image reconstruction was based on angular data measured using an optical fiber position sensor (MR338-Y10C10, Micronor, Camarillo, CA, USA) integrated into the dedicated knee motion device. This optical sensor measured the knee rotation angle with a precision of 0.025°. The optical signals were converted to electrical signals by a controller unit (MR330, Micronor), and then sampled simultaneously with the electrical MRI scanner's sequence trigger signal using a USB-based data acquisition module (RedLab 1208FS, Meilhaus Electronic GmbH). By synchronizing the knee rotation angles with the sequence trigger signal, the acquired radial golden-angle k-space data were then sorted into 2° windows of knee rotation [28]. Image reconstruction was performed using the open-source RIESLING (Radial Interstices Enable Speedy Low-volume imagING) toolbox [29], which is designed to reconstruct non-Cartesian MRI data efficiently. Specifically, the image was reconstructed as a spatially regularized Total Generalized Variation least-squares problem solved using the Alternating Direction Method of Multipliers, where the x-update step used the preconditioned LSMR algorithm [30–35]. A regularization strength of 0.05 was empirically determined to balance noise suppression and edge sharpness.

Fig. 1 shows a series of reconstructed frames from a single dataset, showcasing the progression of knee motion (from a flexed position, to an extended position, back to a flexed position), which were used subsequently as the input data for bone segmentation and tracking.

2.2. Semi-Automated Bone Tracking

For semi-automated tracking of the tibia and femur, the following tracking algorithm was implemented in Python (v.3.11.5). Fig. 2 pro-

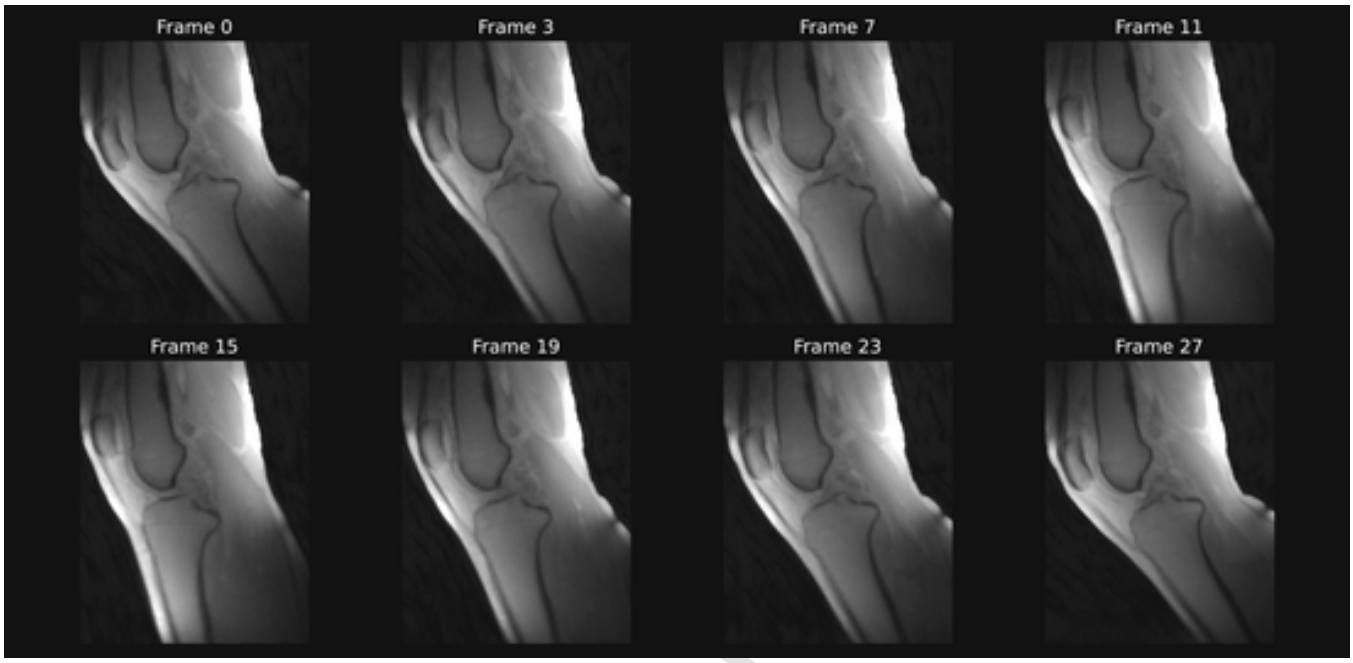

Fig. 1. Reconstructed dynamic CINE MRI frames of knee motion during extension and flexion. Each frame represents a 2° increment in knee angle. Frame 0 shows maximum knee flexion within the confines of the scanner bore, with subsequent frames progressing into extension and returning to flexion in the final frame.

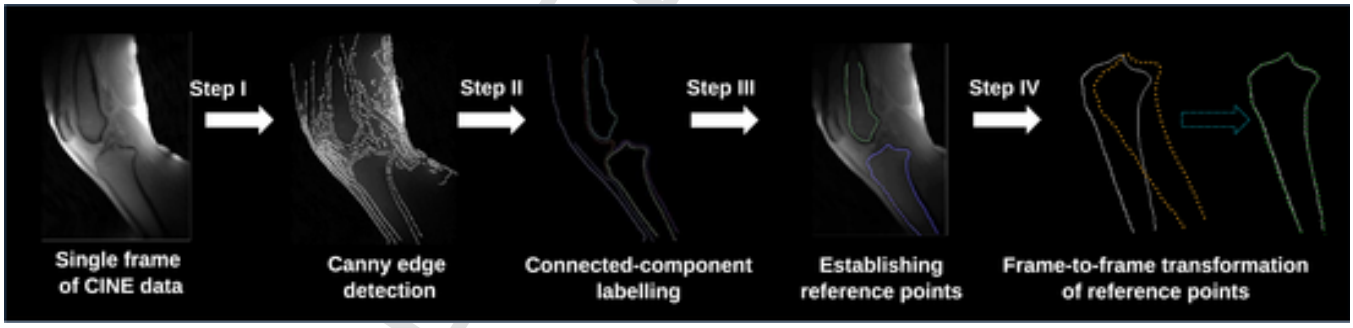

Fig. 2. Schematic overview of the semi-automated pipeline for bone shape tracking. The process includes: (I) Canny edge detection to detect bone edges; (II) Connected-component labeling to isolate cortical bone edges; (III) Establishing reference points along bone edges; and (IV) Computing transformation parameters for frame-to-frame tracking. The final panel shows the reference point transformation for the tibia, illustrating the binary edge (solid white line) with misaligned initial reference points (orange dots) due to bone movement between frames, and subsequently, the aligned points (green dots) after applying the estimated optimal transformation parameters.

vides a schematic overview of the tracking pipeline, consisting of the following steps:

(I) Edge detection: The Canny edge detection algorithm was applied to each frame using the feature module of scikit-image (v0.20.0) to identify the boundaries of the tibia and femur [23]. Parameters such as gradient thresholds and Gaussian blur strength were optimized manually to isolate the bone edges. This step resulted in binary images highlighting the detected edges, including the boundary between cortical and trabecular bone.

(II) Connected-component labeling: Connected-component labeling [24] was performed using the ndimage module of SciPy (v1.11.0) on the binary edge images to isolate specific structural features and distinguish the desired interior cortical bone edges from other detected edges. The labeling algorithm groups adjacent pixels into distinct regions or "components". Through-frame connectivity was used, meaning pixels could be considered part of the same component if they were adjacent (including diagonally) either spatially within a frame or across consecutive frames. This approach ensured that the same bone edge maintained a consistent label throughout the motion sequence, facilitating tracking across frames. In steps I and II, the edge detection and labeling parameters were optimized only once for the given image contrast and resolution and were then applied consistently across all datasets and frames.

(III) Establishing reference points: A set of reference points was defined along the labeled edges of the tibia and femur in the initial flexed frame. This involved identifying the most distal point of the femur and the most proximal point of the tibia, sorting the edge points using a greedy nearest neighbor algorithm [36] and down sampling them to 80 equidistant points via cubic spline interpolation using SciPy's interpolate module [37]. This interpolation process converts the initially discrete edge pixels into continuous coordinate reference points, enabling sub-voxel precision in subsequent transformation and alignment calculations. By establishing these reference points in the initial frame, a template of equidistant points along the bone edges was created that

could be transformed to match the bone positions in subsequent frames, facilitating the tracking of bone movement throughout the motion sequence.

(IV) Transformation computation: Frame-to-frame transformations were computed to align the equidistant reference points of the bone edges. This process assumed rigid body motion described by three parameters: two translations in the sagittal plane and one rotation about the axis perpendicular to the sagittal plane. As illustrated in the final panel of Fig. 2 using the tibia as an example, this involved transforming the initial reference points to match the bone edges in a new position in a target frame. When the transformation parameters were optimally computed, the transformed points aligned perfectly with the binary edge in the new position.

To compute the optimal set of these three parameters, a cost function was defined to quantify the total distance between the transformed reference points (established along the bone edges in the initial frame) and the detected bone edges in the target frame, with a perfect alignment resulting in an output of 0. The goal was to find the combination of transformation parameters that minimize the output of this cost function to effectively identify the optimal way to track the bone edges between consecutive frames. Fig. 3 demonstrates the bone tracking results at different points in the knee motion cycle, showing the segmented bone contours overlaid on the original CINE frames. Videos demonstrating the complete CINE image sequence at physiological speed and the semi-automated tracking results with centroid positions for one participant are available as Supplementary material.

The Nelder-Mead method from the optimize module of SciPy was used to minimize the cost function and obtain the frame-to-frame transformation parameters [38]. To guide the parameter search, constraints were applied based on a priori knowledge of the motion characteristics. For instance, the rotation was restricted to the expected range of frame-to-frame angle increments used during reconstruction, while the translations were limited to incremental values of under 2 mm in each direction to account for the continuous nature of the motion. Once the parameters were obtained for all the frames, any manual segmentation of the bones drawn in the first frame could be automatically transformed to all other frames. The bone alignment error for each frame was computed by dividing the minimized cost function value by the total number of reference points, providing the average distance in millimeters between the transformed reference points and their corresponding detected bone edges in each frame.

The semi-automated approach required manual intervention at two stages: optimization of edge detection parameters for the given image contrast and resolution, and manual selection of labeled components representing the bone edges of interest in the reference frame, performed once per dataset.

2.3. Manual Segmentation and Osteokinematic Analysis

To validate the semi-automated tracking method, manual segmentation was performed for all frames and datasets using the Napari (v.4.16) image processing software [39]. The relative centroid displacements between the tibia and femur were compared between both methods. For manual tracking, the bone segmentation obtained in the first frame was aligned (translated and rotated) manually to match the new bone positions in subsequent frames. Processing time was recorded for both methods, measured from the start of initial frame segmentation to completion of bone tracking across all frames. For manual segmentation, processing times were estimated using a stopwatch during the segmentation process. For the semi-automated approach, processing times were measured on a standard desktop workstation running Python, including both computation steps (edge detection, transformation optimization) and manual interventions (parameter selection, component labelling).

Relative bone positions for both the semi-automated and manual segmentations were quantified by calculating the geometric centroid of each segmented bone region. In the sagittal plane view, the relative displacement between bones was then calculated by subtracting the femoral centroid coordinates from the tibial centroid coordinates. These displacements were measured in the 2D image coordinate system, with the origin at the top left corner and coordinates increasing downward and to the right. This centroid-based approach was chosen as it provides a single-point representation of each bone's position that is less sensitive to local variations in segmentation.

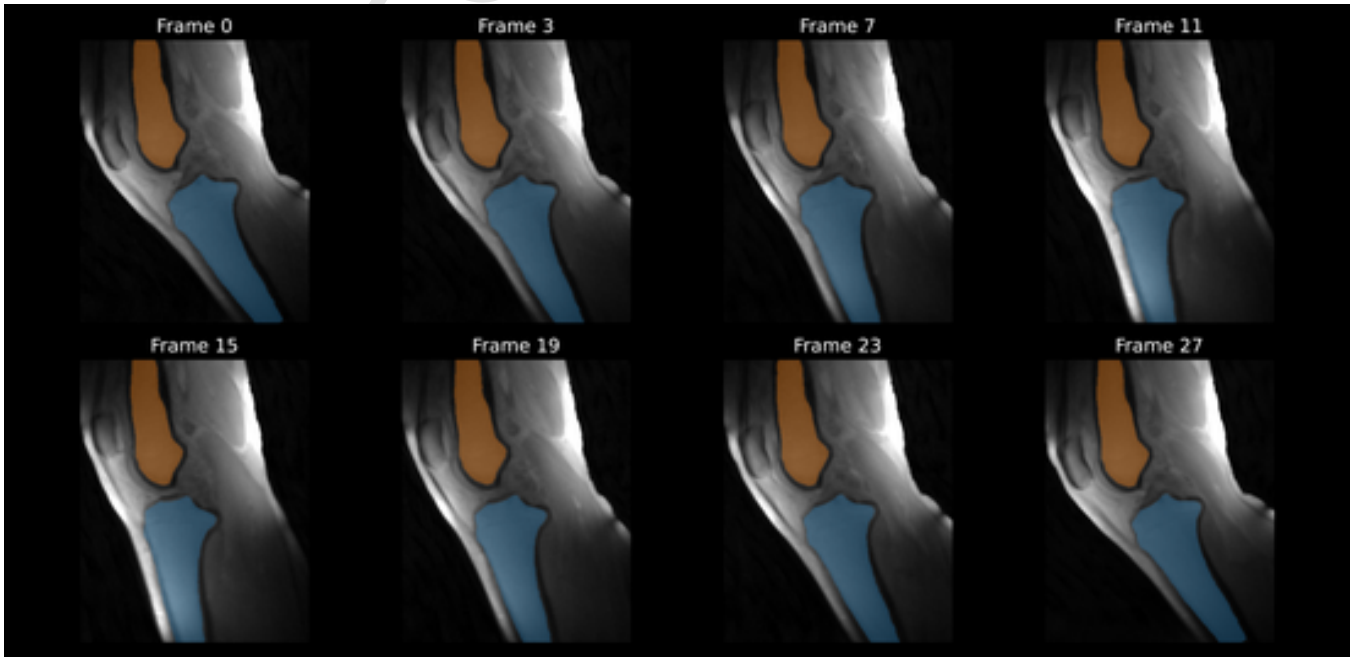

Fig. 3. Example of semi-automated tracking of the femur (orange) and tibia (blue) segmentations overlaid on the base CINE frames at different flexion angles during the knee motion cycle.

To enable comparison across datasets with different knee ranges of motion, the knee flexion angles measured by the optical sensor were normalized to a 'percent extension-flexion cycle' scale. The knee motion cycle was separated into two phases: extension (flexed to extended position) and flexion (extended to flexed position). Each phase was normalized from 0% to 100%. Due to inter-participant variations in frame counts resulting from differences in achieved knee range of motion, the normalized flexion cycle data were binned into 10% intervals (0-10%, 10-20%, etc.), with displacement values averaged within each bin across all datasets.

The tracking accuracy of the algorithm was evaluated using the cost function described in section 2.2, which quantified the summed distance between the transformed reference points and the detected bone edges. The cost function value divided by the total number of reference points provided an average alignment error in millimeters for each bone in each frame.

3. Results

The semi-automated tracking algorithm successfully tracked both the tibial and femoral bone edges throughout the motion cycle for all five participants. The number of reconstructed frames varied among participants based on their achieved knee range of motion, which ranged from 30° to 46°.

When averaged across both bones, all frames, and all datasets, the alignment error between the transformed reference points and detected bone edges was 0.40 ± 0.02 mm. The segmentation time required by the semi-automated approach was less than 5 minutes per dataset, compared to approximately 15 minutes per dataset using the manual approach.

Fig. 4 presents the results of the quantitative osteokinematic analysis of relative bone motion, which revealed consistent displacement patterns across all participants. The horizontal displacement of the tibial centroid relative to the femoral centroid showed a linear trend during both the knee extension and flexion phases, ranging from approximately 8 mm to 28 mm through the motion cycle. The vertical

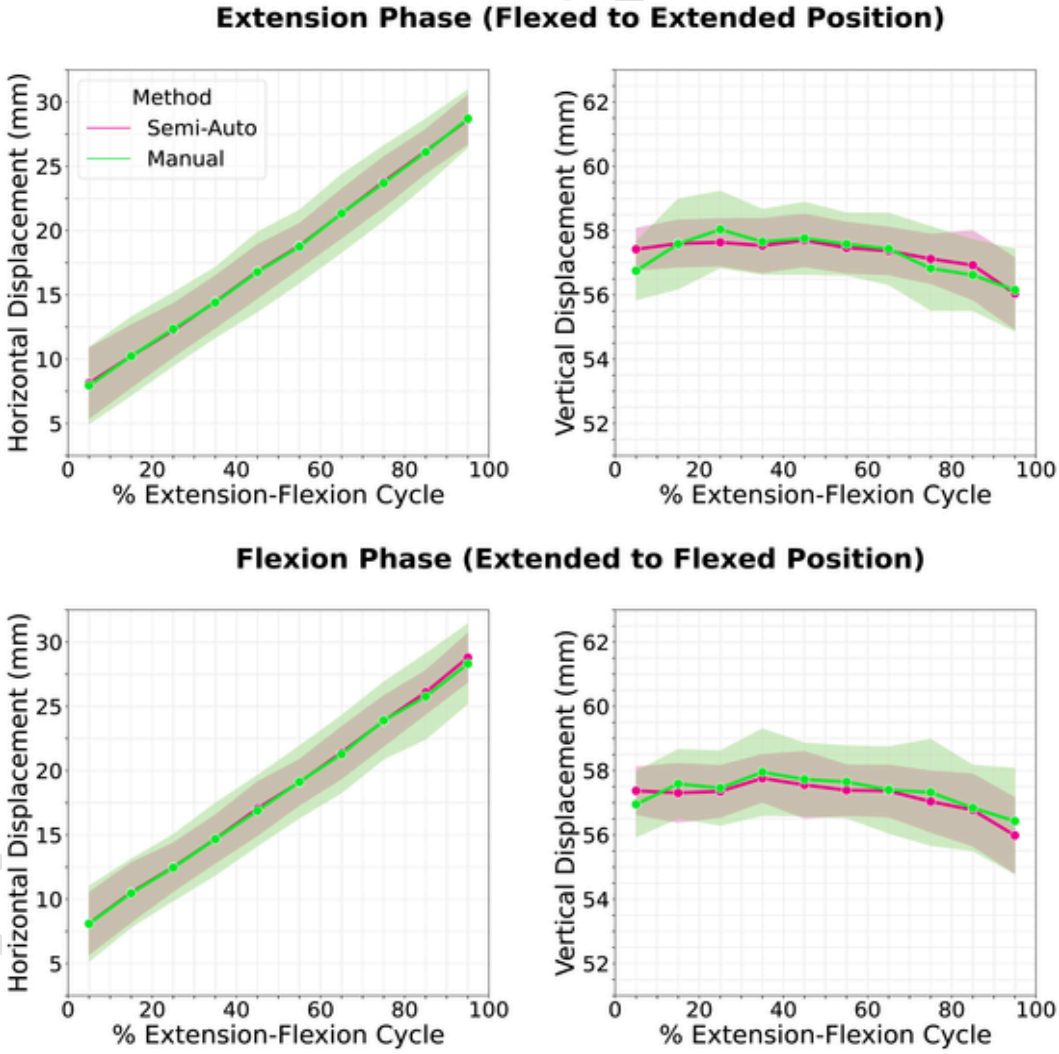

Fig. 4. Comparison of relative bone motion of the tibia with respect to the femur during knee extension and flexion. The top row shows the knee extension phase (flexed to extended position), while the bottom row shows the knee flexion phase (extended to flexed position). The left panels depict horizontal tibial displacement, while the right panels depict vertical tibial displacement. Relative bone displacement was calculated by subtracting the femoral centroid coordinates from those of the tibia (semi-automated segmentation in pink; manual segmentation in lime-green). Shaded regions indicate standard deviations around group means. These displacements were measured in the 2D image coordinate system, with the origin at the top left corner and coordinates increasing downward and to the right.

displacement remained relatively constant around 57 mm. Both semi-automated and manual methods demonstrated similar knee motion patterns, with the semi-automated method showing consistently smaller variability (SDs) across all measurements. For horizontal displacement, the semi-automated method demonstrated lower variability (SDs of 1.7–2.7 mm) compared to the manual method (SDs of 2.2–3.3 mm). Similarly, for vertical displacement, the semi-automated method showed lower variability (SDs of 0.7–1.2 mm) compared to the manual method (SDs of 0.9–1.7 mm).

4. Discussion

The results demonstrate the technical feasibility of our semi-automated bone tracking approach for analyzing knee motion from dynamic CINE MRI data during flexion and extension. The method achieved an average alignment error of 0.40 ± 0.02 mm between the discretized bone edge from the previous frame (80 reference points) and the continuous Canny edge of the next frame, while significantly reducing processing time compared to manual segmentation. The smaller variability (SDs) observed with the semi-automated method suggests improved measurement consistency compared to manual tracking, likely due to the algorithmic approach being less susceptible to human variability in frame-to-frame segmentation.

The semi-automated method successfully quantified 2D knee motion patterns in the sagittal plane across all participants. The osteokinematic measurements revealed consistent trends: a systematic, linear change in horizontal bone displacement (8–28 mm) through the knee extension-flexion cycle, and a relatively stable vertical bone displacement (57 ± 2 mm). The reconstruction of CINE frames at 2° windows of knee rotation was selected as it provided sufficient temporal sampling density for osteokinematic analysis while keeping the number of frames computationally manageable. While image reconstruction at smaller angular windows would yield more data points in the displacement curves, it would increase processing time without substantially improving the characterization of bone motion patterns. Smaller knee rotation windows would also reduce image signal-to-noise ratio and could lead to under-sampling artifacts that have the potential to interfere with edge detection. The consistency of the osteokinematic analysis between participants demonstrates the method's ability to capture reproducible motion patterns, though establishing normative ranges would require larger population studies.

The ability of the semi-automated method to precisely track bone motion could be particularly valuable for studying conditions that alter normal knee mechanics. For instance, knee ligament injuries can affect joint stability and lead to increased laxity [40], potentially resulting in altered tibiofemoral movement patterns during functional activities, as shown in individuals with anterior cruciate ligament deficiency [41]. Unlike passive clinical tests such as the anterior-posterior drawer test, our method captures joint behavior during active, muscle-driven flexion-extension, potentially revealing functional instability patterns with greater physiological relevance. The precision and efficiency of the presented method make it a promising tool for comparative analyses between normal and pathological knee osteokinematics, though further validation is required for meaningful clinical interpretation in specific patient cohorts and correlation with traditional clinical assessments.

Several technical aspects of our approach contribute to its potential clinical utility. The method operates directly on dynamic MRI data without requiring additional static reference scans, streamlining the workflow and shortening the acquisition time. The semi-automated nature of the bone tracking reduces processing time while maintaining high segmentation precision compared to manual approach, making it more practical for both research and clinical applications.

Despite these advantages, a limitation of the current 2D approach is sensitivity to through-plane motion. While the knee motion device was designed to constrain movement to the sagittal plane, through-plane motion remains a potential source of error. This limitation also led us to exclude the patella from our analysis despite its visibility in the sagittal images, as it undergoes significant through-plane motion during flexion-extension that is incompatible with our 2D tracking approach. In cases where significant through-plane motion occurs, the bone appearances in the fixed sagittal slice change, resulting in elevated cost function values that indicate compromised tracking accuracy. Future work could address this limitation by extending the method to 3D acquisitions.

Furthermore, the knee range of motion achievable in closed-bore MRI systems is limited by the bore diameter and the length of the lower leg, precluding the assessment of deep (full) knee flexion. In the current study, the bore diameter was 60 cm and allowed for knee flexion angles between 30° and 46°. Open-bore MRI systems would be better suited to perform full knee range of motion examinations [42], on which the methods presented in this report should also work.

5. Conclusion

A novel semi-automated method was developed and validated for tracking bone motion using 2D sagittal plane CINE MRI images acquired during controlled knee flexion and extension. The method significantly reduces processing time compared to manual segmentation, while improving osteokinematic consistency. These advantages make the semi-automated approach particularly attractive for studying both normal and pathological knee motion patterns in research and clinical settings.

Funding Information

This research was funded by the German Research Foundation (DFG – Deutsche Forschungsgemeinschaft, BR 6698/1-1, KR 4783/2-1). The funding source had no role in the design of this study; in the collection, analysis and interpretation of data; in the writing of the article; and in the decision to submit the article for publication.

CRediT authorship contribution statement

A. Nepal: Writing – original draft, Visualization, Validation, Software, Methodology, Investigation, Formal analysis, Data curation. **N.M. Brisson:** Writing – review & editing, Funding acquisition, Conceptualization. **T.C. Wood:** Writing – review & editing, Software. **G.N. Duda:** Writing – review & editing. **J.R. Reichenbach:** Writing – review & editing, Supervision. **M. Krämer:** Writing – review & editing, Visualization, Supervision, Software, Project administration, Funding acquisition, Conceptualization.

Declaration of competing interest

The authors declare that they have no known competing financial interests or personal relationships that could have appeared to influence the work reported in this paper.

Appendix A. Supplementary data

Supplementary data to this article can be found online at https://doi.org/10.1016/j.zemedi.2025.06.005.

References

[1] Heiser R, O'Brien VH, Schwartz DA. The use of joint mobilization to improve clinical outcomes in hand therapy: A systematic review of the literature. J Hand Ther 2013;26:297–311. https://doi.org/10.1016/j.jht.2013.07.004.

[2] Postolka B, Taylor WR, Dätwyler K, Heller MO, List R, Schütz P. Interpretation of natural tibio-femoral kinematics critically depends upon the kinematic analysis approach: A survey and comparison of methodologies. J Biomech 2022;144:111306. https://doi.org/10.1016/j.jbiomech.2022.111306.

[3] Tashman S, Anderst W. In-vivo measurement of dynamic joint motion using high speed biplane radiography and CT: application to canine ACL deficiency. J Biomech Eng 2003;125:238–45. https://doi.org/10.1115/1.1559896.

[4] D'Lima DD, Patil S, Steklov N, Colwell CW. The 2011 ABJS Nicolas Andry Award: 'Lab'-in-a-knee: in vivo knee forces, kinematics, and contact analysis. Clin Orthop Relat Res 2011;469:2953–70. https://doi.org/10.1007/s11999-011-1916-9.

[5] Tashman S, Kopf S, Fu FH. The Kinematic basis of anterior cruciate ligament reconstruction. Operative Techniques in Sports Medicine 2008;16:116–8. https://doi.org/10.1053/j.otsm.2008.10.005.

[6] Astephen JL, Deluzio KJ, Caldwell GE, Dunbar MJ. Biomechanical changes at the hip, knee, and ankle joints during gait are associated with knee osteoarthritis severity. J Orthop Res 2008;26:332–41. https://doi.org/10.1002/jor.20496.

[7] Kaufman KR, Hughes C, Morrey BF, Morrey M, An KN. Gait characteristics of patients with knee osteoarthritis. J Biomech 2001;34:907–15. https://doi.org/10.1016/S0021-9290(01)00036-7.

[8] Andriacchi TP, Koo S, Scanlan SF. Gait mechanics influence healthy cartilage morphology and osteoarthritis of the knee. J Bone Joint Surg Am 2009;91(Suppl 1): 95–101. https://doi.org/10.2106/JBJS.H.01408.

[9] Sharma L, Lou C, Felson DT, Dunlop DD, Kirwan-Mellis G, Hayes KW, et al. Laxity in healthy and osteoarthritic knees. Arthritis Rheum 1999;42:861–70. https://doi.org/10.1002/1529-0131(199905)42:5<861::AID-ANR4>3.0.CO;2-N.

[10] Lohmander LS, Englund PM, Dahl LL, Roos EM. The long-term consequence of anterior cruciate ligament and meniscus injuries: osteoarthritis. Am J Sports Med 2007;35:1756–69. https://doi.org/10.1177/0363546507307396.

[11] Sharma L. The role of proprioceptive deficits, ligamentous laxity, and malalignment in development and progression of knee osteoarthritis. J Rheumatol Suppl 2004;70:87–92.

[12] Van Rossom S, Wesseling M, Smith CR, Thelen DG, Vanwanseele B, Dieter VA, et al. The influence of knee joint geometry and alignment on the tibiofemoral load distribution: A computational study. Knee 2019;26:813–23. https://doi.org/10.1016/j.knee.2019.06.002.

[13] Arakgi ME, Getgood A. Mechanical Malalignment of the Knee Joint. Evidence-Based Management of Complex Knee Injuries 2022; :66–76. DOI: 10.1016/B978-0-323-71310-8.00005-0

[14] d'Entremont AG, Nordmeyer-Massner JA, Bos C, Wilson DR, Pruessmann KP. Do dynamic-based MR knee kinematics methods produce the same results as static methods? Magnetic Resonance in Med 2013;69:1634–44. https://doi.org/10.1002/mrm.24425.

[15] Conconi M, De Carli F, Berni M, Sancisi N, Parenti-Castelli V, Monetti G. In-Vivo quantification of knee Deep-Flexion in physiological loading condition trough dynamic MRI. Appl Sci 2023;13:629. https://doi.org/10.3390/app13010629.

[16] Draper CE, Besier TF, Santos JM, Jennings F, Fredericson M, Gold GE, et al. Using real-time MRI to quantify altered joint kinematics in subjects with patellofemoral pain and to evaluate the effects of a patellar brace or sleeve on joint motion. J Orthop Res 2009;27:571–7. https://doi.org/10.1002/jor.20790.

[17] Kaiser JM, Vignos MF, Kijowski R, Baer G, Thelen DG. Effect of loading on in vivo tibiofemoral and patellofemoral kinematics of healthy and ACL-Reconstructed knees. Am J Sports Med 2017;45:3272–9. https://doi.org/10.1177/0363546517724417.

[18] Brossmann J, Muhle C, Schröder C, Melchert UH, Büll CC, Spielmann RP, et al. Patellar tracking patterns during active and passive knee extension: evaluation with motion-triggered cine MR imaging. Radiology 1993;187:205–12. https://doi.org/10.1148/radiology.187.1.8451415.

[19] Seisler AR, Sheehan FT. Normative three-dimensional patellofemoral and tibiofemoral kinematics: a dynamic, in vivo study. IEEE Trans Biomed Eng 2007; 54:1333–41. https://doi.org/10.1109/TBME.2007.890735.

[20] Behnam AJ, Herzka DA, Sheehan FT. Assessing the accuracy and precision of musculoskeletal motion tracking using cine-PC MRI on a 3.0T platform. J Biomech 2011;44:193–7. https://doi.org/10.1016/j.jbiomech.2010.08.029.

[21] Kaiser J, Bradford R, Johnson K, Wieben O, Thelen DG. Measurement of tibiofemoral kinematics using highly accelerated 3D radial sampling. Magnetic Resonance in Med 2013;69:1310–6. https://doi.org/10.1002/mrm.24362.

[22] Della Croce U, Leardini A, Chiari L, Cappozzo A. Human movement analysis using stereophotogrammetry: assessment of anatomical landmark misplacement and its effects on joint kinematics. Gait Posture 2005;21:226–37. https://doi.org/10.1016/j.gaitpost.2004.05.003.

[23] Canny J. A computational approach to edge detection. IEEE Trans Pattern Anal Mach Intell 1986;PAMI-8:679–98. https://doi.org/10.1109/TPAMI.1986.4767851.

[24] Dillencourt MB, Samet H, Tamminen M. A general approach to connected-component labeling for arbitrary image representations. J ACM 1992;39:253–80. https://doi.org/10.1145/128749.128750.

[25] Brisson NM, Krämer M, Krahl LAN, Schill A, Duda GN, Reichenbach JR. A novel multipurpose device for guided knee motion and loading during dynamic magnetic resonance imaging. Zeitschrift für Medizinische Physik 2022;32:500–13. https://doi.org/10.1016/j.zemedi.2021.12.002.

[26] Winkelmann S, Schaeffter T, Koehler T, Eggers H, Doessel O. An optimal radial profile order based on the golden ratio for time-resolved MRI. IEEE Trans Med Imaging 2007;26:68–76. https://doi.org/10.1109/TMI.2006.885337.

[27] Krämer M, Herrmann K, Biermann J, Reichenbach JR. Retrospective reconstruction of cardiac cine images from golden-ratio radial MRI using one-dimensional navigators. Magn Reson Imaging 2014;40:413–22. https://doi.org/10.1002/jmri.24364.

[28] Aleksiev M, Krämer M, Brisson NM, Maggioni MB, Duda GN, Reichenbach JR. High-resolution CINE imaging of active guided knee motion using continuously acquired golden-angle radial MRI and rotary sensor information. Magn Reson Imaging 2022;92:161–8. https://doi.org/10.1016/j.mri.2022.06.015.

[29] Wood T, Ljungberg E, Wiesinger F. Radial interstices enable speedy low-volume imaging. JOSS 2021;6:3500. https://doi.org/10.21105/joss.03500.

[30] Boyd S. Distributed optimization and statistical learning via the alternating direction method of multipliers. FNT Mach Learn 2010;3:1–122. https://doi.org/10.1561/2200000016.

[31] Bredies K, Kunisch K, Pock T. Total generalized variation. SIAM J Imaging Sci 2010;3:492–526. https://doi.org/10.1137/090769521.

[32] Ong F, Uecker M, Lustig M. Accelerating Non-Cartesian MRI reconstruction convergence using k-Space preconditioning. IEEE Trans Med Imaging 2020;39: 1646–54. https://doi.org/10.1109/TMI.2019.2954121.

[33] Montoison A, Orban D. Krylov.jl: A Julia basket of hand-picked Krylov methods. JOSS 2023;8:5187. https://doi.org/10.21105/joss.05187.

[34] Fong DCL, Saunders M. LSMR: An iterative algorithm for sparse least-squares problems. SIAM J Sci Comput 2011;33:2950–71. https://doi.org/10.1137/10079687X.

[35] TC. Wood, Algorithms for Least-Squares Noncartesian MR Image Reconstruction. 2022; DOI: 10.48550/ARXIV.2212.06471

[36] A. Hinneburg, C.C. Aggarwal, D.A. Keim, What is the nearest neighbor in high dimensional spaces? Proc of the 26th Internat Conference on Very Large Databases, Cairo, Egypt, 2000 2000; :506–15

[37] De Boor C. A Practical Guide to Splines. 1978;27. https://doi.org/10.1007/978-1-4612-6333-3.

[38] Nelder JA, Mead R. A simplex method for function minimization. Comput J 1965;7:308–13. https://doi.org/10.1093/comjnl/7.4.308.

[39] Sofroniew N, Lambert T, Evans K, Nunez-Iglesias J, Bokota G, Winston P, et al. napari: a multi-dimensional image viewer for. Python. 2022. https://doi.org/10.5281/ZENODO.6598542.

[40] Shimizu T, Cheng Z, Samaan MA, Tanaka MS, Souza RB, Li X, et al. Increases in joint laxity after anterior cruciate ligament reconstruction are associated with sagittal biomechanical asymmetry. Arthroscopy 2019;35:2072–9. https://doi.org/10.1016/j.arthro.2019.01.050.

[41] Barrance PJ, Williams GN, Snyder-Mackler L, Buchanan TS. Altered knee kinematics in ACL-deficient non-copers: a comparison using dynamic MRI. J Orthop Res 2006;24:132–40. https://doi.org/10.1002/jor.20016.

[42] Draper CE, Santos JM, Kourtis LC, Besier TF, Fredericson M, Beaupre GS, et al. Feasibility of using real-time MRI to measure joint kinematics in 1.5T and open-bore 0.5T systems. Magn Reson Imaging 2008;28:158–66. https://doi.org/10.1002/jmri.21413.